Int. J. Heat Mass Transfer. Vol. 34, No. 9, pp. 2423–2427, 1991
Printed in Great Britain

0017–9310/91 $3.00 + 0.00
© 1991 Pergamon Press plc

TECHNICAL NOTES

Double diffusive convection in a cavity under a vertical solutal gradient and a horizontal temperature gradient

JIN WOOK LEE and JAE MIN HYUN†

Department of Mechanical Engineering, Korea Advanced Institute of Science and Technology, P.O. Box 150, Cheong Ryang, Seoul, Korea

(*Received* 21 *September* 1990)

1. INTRODUCTION

DOUBLE diffusive convection in a confined space has been extensively investigated at late. One striking feature of this flow field is the emergence of the layered structure under certain physical conditions. The layers are separated by very thin interfaces, and the density field varies rapidly across the interfaces.

The early laboratory experiments produced this layered structure by differentially heating the vertical sidewalls of a cavity, which contained a liquid solution with a pre-existing stable stratification [1, 2]. The quantitative measurements by Chen *et al.* [3] led to an identification of the critical Rayleigh number Ra_c, beyond which a series of layers was seen to extend from the heated sidewall. Further elaborate undertakings, both experimental and numerical, have illuminated the prominent characteristics of the layered structure that is attainable in double diffusive convection in an enclosure [4–6]. The significance of the 'heated-by-the-sidewall' flow configuration, in the general context by buoyant flow systems, was emphasized by Ostrach [7]. Recently, numerical studies [8] clearly demonstrated that the horizontal rolls propagated into the interior from the heated sidewall in a double diffusive system.

The afore-mentioned works, in particular, the experimental efforts, have considerably deepened the understanding of the essential dynamics of double diffusive convective flows. It is important, however, to point out that, in the majority of the previous experiments, the entire boundary walls of the container were assumed to be impervious to mass transfer. This condition at the bounding walls was adopted mainly because of the practical considerations in fabricating an experimental container. In the laboratory, it is relatively easy to construct the walls of the enclosure by metallic plates; in this case, the walls are effectively insulated for mass transport. Consequently, in the experiments performed by using this kind of laboratory apparatus, the pre-existing solute stratification is bound to be destroyed as time progresses. Since there are no sources or sinks of solute on the boundary walls, the initially-imposed solutal stratification vanishes ultimately by the action of the cellular convection induced by the thermal buoyancy.

Very recently, an experimental rig was devised in which the horizontal walls were made of membranes, thus allowing solute transfer across the system boundaries [9]. Using this experimental set-up, the time-dependent flow behaviour was monitored in a double diffusive system in which a constant solute difference was maintained across the entire height of the container. As noted previously, this represents an interesting experimental condition in the sense that the system is subject to the laterally-oriented heating as well as the vertically-directed solutal gradient. Ostrach [7] stressed that the basic properties of buoyant flows are extremely sensitive to the magnitudes and orientations of the external forces. The flow configuration in the present study falls into the category in which the vectors of the externally-applied temperature gradient and solutal gradient are perpendicular to each other [7]. The observations of ref. [9] led to a qualitative identification of four distinct flow regimes in a near-steady state; the principal deciding parameter is the buoyancy ratio $R_\rho (\equiv R_s/R_t)$, R_t and R_s being the thermal and solutal Rayleigh numbers. The regime diagram in ref. [9] ascertains that, as R_ρ encompasses a broad range of values, four distinguishing flow patterns are discernible: the unicell flow; the fully-developed layered-structure flow; the layered-structure pattern together with a stagnant interior; and the essentially-motionless flow structure.

In the present note the experimental findings of ref. [9] regarding the double diffusive convection in a rectangular cavity are verified. The primary object is to secure high-resolution numerical solutions to the governing full Navier–Stokes equations for the afore-stated flow geometry. The essence of this flow configuration is that the externally-supplied buoyancy sources are the lateral heating and the vertically-applied solutal gradient. The numerical solutions are acquired over a wide range of the buoyancy ratio $R_\rho = 3.0$–50.0. The salient flow characteristics will be illuminated by inspecting the numerical results; the wealth and breadth of the numerical solutions provide the additional details which are not readily available by experiments alone. The large-time behaviour of flow will be scrutinized. These numerical data at large times are shown to be qualitatively consistent with the earlier experimental observations of ref. [9]; this confirms the existence of several distinct flow regimes as R_ρ covers a broad range of values. By post-processing the numerical results describing the thermal fields, the heat transfer rate on the vertical sidewall is computed. These should yield useful base data for heat and mass transfer correlations in double diffusive convection in a confined space.

2. THE MODEL

The governing equations are the full, time-dependent Navier–Stokes equations with the Boussinesq-fluid assumption incorporated. These equations, expressed in properly non-dimensionalized form and using standard notation, are

$$\frac{\partial U}{\partial X} + \frac{\partial V}{\partial Y} = 0$$

$$\frac{\partial U}{\partial \tau} + \frac{\partial}{\partial X}(UU) + \frac{\partial}{\partial Y}(VU) = -\frac{\partial P}{\partial X} + Pr\left(\frac{\partial^2 U}{\partial X^2} + \frac{\partial^2 U}{\partial Y^2}\right)$$

$$\frac{\partial V}{\partial \tau} + \frac{\partial}{\partial X}(UV) + \frac{\partial}{\partial Y}(VV) = -\frac{\partial P}{\partial Y} + Pr\left(\frac{\partial^2 V}{\partial X^2} + \frac{\partial^2 V}{\partial Y^2}\right) + Pr\,(R_t T - R_s S)$$

† Author to whom all correspondence should be addressed.

NOMENCLATURE

Ar	aspect ratio, H/L
C_h	dimensional concentration at the high-concentration bottom wall
C_l	dimensional concentration at the low-concentration top wall
ΔC	concentration difference, $C_h - C_l$
D	mass diffusivity
g	gravity
H	height of cavity
L	width of cavity
Le	Lewis number, κ/D
Nu	local Nusselt number
P	non-dimensional pressure
p	dimensional pressure
Pr	Prandtl number, ν/κ
R_s	solutal Rayleigh number, $g\beta_s\Delta CL^3/\kappa\nu$
R_t	thermal Rayleigh number, $g\beta_t\Delta\theta L^3/\kappa\nu$
R_ρ	buoyancy ratio, $\beta_s\Delta C/\beta_t\Delta\theta$
S	non-dimensional concentration
T	non-dimensional temperature
t	dimensional time
U	non-dimensionalized horizontal velocity component
u	dimensional horizontal velocity component
V	non-dimensionalized vertical velocity component
v	dimensional vertical velocity component
X	non-dimensional horizontal coordinate
x	dimensional horizontal coordinate
Y	non-dimensional vertical coordinate
y	dimensional vertical coordinate.

Greek symbols

β_s	coefficient of volumetric expansion with concentration
β_t	coefficient of volumetric expansion with temperature
θ_h	dimensional temperature at the high-temperature sidewall
θ_l	dimensional temperature at the low-temperature sidewall
$\Delta\theta$	temperature difference, $\theta_h - \theta_l$
κ	thermal diffusivity
ν	kinematic viscosity
ρ	dimensional density
τ	non-dimensional time
ψ	non-dimensional stream function.

$$\frac{\partial T}{\partial \tau} + \frac{\partial}{\partial X}(UT) + \frac{\partial}{\partial Y}(VT) = \left(\frac{\partial^2 T}{\partial X^2} + \frac{\partial^2 T}{\partial Y^2}\right)$$

$$\frac{\partial S}{\partial \tau} + \frac{\partial}{\partial X}(US) + \frac{\partial}{\partial Y}(VS) = -\frac{1}{Le}\left(\frac{\partial^2 S}{\partial X^2} + \frac{\partial^2 S}{\partial Y^2}\right).$$

In the above, the dimensionless quantities are defined as

$$U = [u/(\kappa/L)], \quad V = [v/(\kappa/L)], \quad X = x/L,$$
$$Y = y/L, \quad \tau = [t/(L^2/\kappa)],$$
$$P = p/(\rho\kappa^2/L^2), \quad \Delta\theta = \theta_h - \theta_l,$$
$$\Delta C = C_h - C_l, \quad T = (\theta - \theta_l)/\Delta\theta,$$
$$S = (C - C_l)/\Delta C, \quad Pr = \nu/\kappa, \quad Le = \kappa/D, \quad Ar = H/L,$$
$$R_t = g\beta_t\Delta\theta L^3/\kappa\nu, \quad R_s = g\beta_s\Delta CL^3/\kappa\nu,$$
$$R_\rho = (\beta_s\Delta C)/(\beta_t\Delta\theta) = R_s/R_t.$$

Clearly the relevant non-dimensional parameters are: the Prandtl number, Pr; the Lewis number, Le; the thermal Rayleigh number, R_t; the solutal Rayleigh number, R_s; and the cavity aspect ratio, Ar.

Figure 1 is a schematic of the configuration, illustrating the Cartesian coordinates (x, y) and the corresponding velocity components (u, v). As ascertained earlier, at the initial state, the fluid is at rest and at uniform temperature ($T = 0$) in the entire cavity. However, the fluid is stably stratified due to a pre-existing, vertically-linear solutal stratification. The fluid motions are initiated at the initial instant $\tau = 0$ by giving a step change in the temperature of the left vertical sidewall ($X = 0$) to $T = 1$. This creates an externally-applied horizontal temperature gradient on the system. The vertical walls are impermeable to solute, i.e. $\partial S/\partial X = 0$. As remarked previously, the crux of the present problem is that the solutal concentration difference is maintained between the top and bottom horizontal boundaries. The horizontal walls are thermally insulated. The tasks here are to portray the ensuing flow, temperature and solutal fields inside the container. In accordance with the problem statement, the appropriate initial and boundary conditions can be summarized as

$$U = V = T = 0, \quad S = 1 - Y/Ar \quad \text{at } \tau = 0;$$
$$U = V = 0 \quad \text{on all solid boundaries};$$
$$S = 1 \quad \text{on } Y = 0, \quad S = 0 \quad \text{on } Y = Ar;$$
$$T = 1 \quad \text{on } X = 0, \quad T = 0 \quad \text{on } X = 1;$$
$$\frac{\partial T}{\partial Y} = 0 \quad \text{on } Y = 0, \quad Ar;$$
$$\frac{\partial S}{\partial X} = 0 \quad \text{on } X = 0, 1.$$

The numerical techniques to solve the above equations have been well established. We have chosen an amended version of the well-known SIMPLER algorithm, which was originally developed by Patankar [10]. The SIMPLER is based on an iterative method, and the convergence criteria

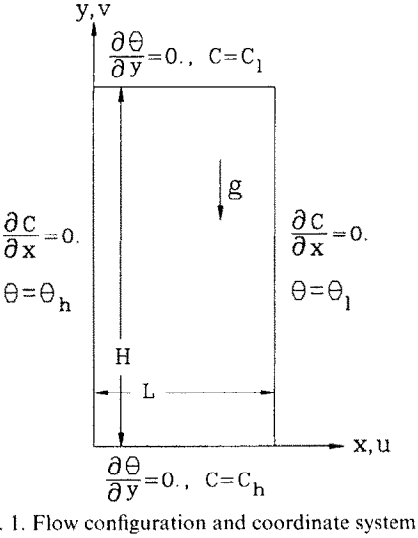

FIG. 1. Flow configuration and coordinate system.

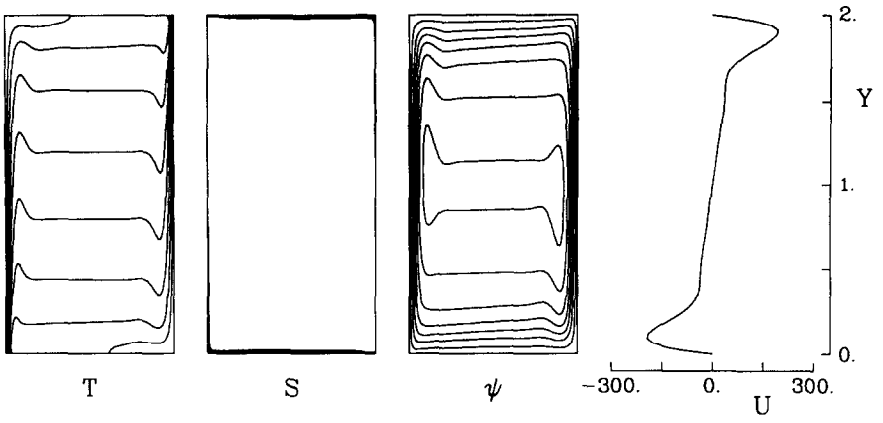

FIG. 2. Plots of isotherms (T), iso-solutal lines (S), stream functions (ψ), and vertical profile of horizontal velocity (U) at mid-width. Conditions are $R_t = 10^7$ and $R_\rho = 3.0$. Values for ψ are, from the boundary to the interior, $0.05\psi_{min}$, $0.20\psi_{min}$, $0.35\psi_{min}$, $0.50\psi_{min}$, $0.65\psi_{min}$, $0.80\psi_{min}$ and $0.95\psi_{min}$. Values for isotherms are, from left to right, 0.889, 0.778, 0.667, 0.556, 0.444, 0.333, 0.222 and 0.111. Values for iso-solutal lines are, from bottom to top, 0.889, 0.778, 0.667, 0.556, 0.444, 0.333, 0.222 and 0.111. Maximum and minimum values of ψ are $\psi_{min} = -0.5792 \times 10^2$ and $\psi_{max} = 0.0$.

are needed. In the present study, we have adopted the following convergence criteria at each time step:

$$\frac{\left|\left(\frac{\partial U}{\partial X} + \frac{\partial Y}{\partial Y}\right)_{i,j}\right|_{max}}{|U_{i,j}|_{max}} < \varepsilon_1, \quad \left|\frac{\phi_{i,j}^{k+1} - \phi_{i,j}^{k}}{\phi_{ij}^{k+1}}\right|_{max} < \varepsilon_2$$

where ε_1 and ε_2 are typically 10^{-6} and 10^{-4}, respectively, ϕ indicates the physical variable of interest, and superscript k denotes the iteration index. The grid net was highly stretched in the vicinity of the solid walls to improve resolution of the boundary layers. The typical grid points in the present study were (51×85).

3. RESULTS AND DISCUSSION

A set of comprehensive and systematically-organized numerical solutions was acquired to delineate the proper flow characteristics at high Rayleigh numbers of the system. The Prandtl number and the Lewis number were set at $Pr = 7.0$ and $Le = 100.0$, to model salt water. The major impetus of the study is to characterize the flow regimes as the buoyancy ratio R_ρ scans a broad range. In the actual computations, the thermal Rayleigh number was fixed at $R_t = 10^7$ and R_s was allowed to vary; the scope of $R_\rho (\equiv R_s/R_t)$ was 3.0–50.0. The aspect ratio was set at $Ar = 2.0$ to simulate closely the experiments of ref. [9].

The main elements of the discussion are concerned with the description of the large-time behaviour of flow. It is recalled that there are reservoirs of solute of different strengths at the horizontal walls. Classifications of the flow patterns will be shown to be qualitatively consistent with the prior experimental observations [9].

In the present work, the time-marching calculations were continued until quasi-steady solutions were reached. The criterion used was

$$|(\phi_{i,j}^{k+1} - \phi_{i,j}^{k})/\phi_{i,j}^{k+1}| < \varepsilon$$

where ε is the pre-assigned value, typically 10^{-6}; ϕ indicates the physical variable, and superscript k denotes the index of the time level. As expected, the flow variables tend to change rather slowly at large times.

The eminent features characteristic of the flows of small buoyancy ratio are exemplified in Fig. 2 (at $R_\rho = 3.0$). Obvi-

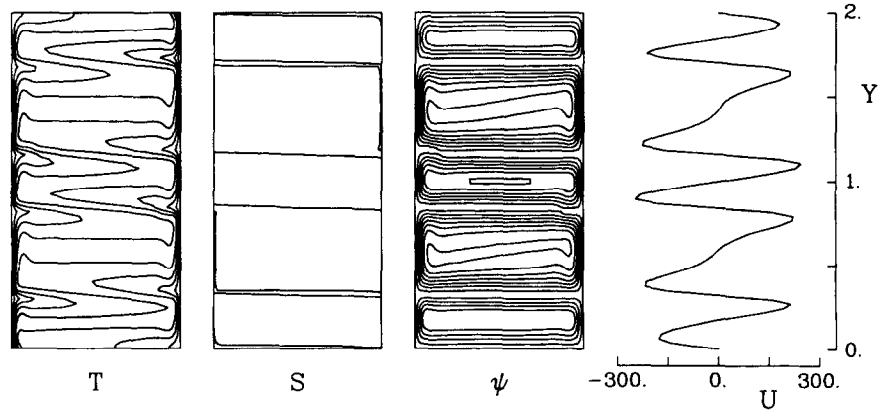

FIG. 3. Plots of isotherms (T), iso-solutal lines (S), stream functions (ψ), and vertical profile of horizontal velocity (U) at mid-width. Conditions are $R_t = 10^7$ and $R_\rho = 15.0$. Values for T, S and ψ are the same as in Fig. 2. Maximum and minimum values of ψ are $\psi_{min} = -0.2987 \times 10^2$ and $\psi_{max} = 0.8367 \times 10^{-1}$.

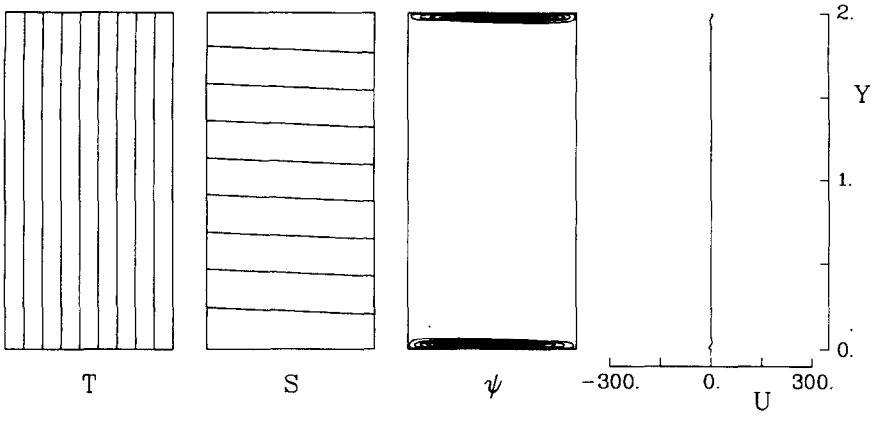

FIG. 4. Plots of isotherms (T), iso-solutal lines (S), stream functions (ψ), and vertical profile of horizontal velocity (U) at mid-width. Conditions are $R_t = 10^7$ and $R_\rho = 50.0$. Values for T, S and ψ are the same as in Fig. 2. Maximum and minimum values of ψ are $\psi_{min} = -0.9734 \times 10^{-1}$ and $\psi_{max} = 0.1859 \times 10^{-1}$.

ously, thermal convection is dominant, and the global flow structure is akin to a single diffusive, purely thermal convection (e.g. see ref. [11]). The thermal field in the interior core exhibits a nearly-linear vertical stratification. The iso-solutal lines are highly crowded in extremely thin regions adjacent to the horizontal walls. The variations of solutal concentration are very large only in these thin horizontal near-wall regions; in the bulk of the interior core, the solutal field is well mixed and is at the mean value $S = 0.5$. In the whole cavity, the unicell flow, dominated by the convection caused by thermal buoyancy, is discernible.

The numerical results for an intermediate value of R_ρ are depicted in Fig. 3 (for $R_\rho = 15.0$). The thermal and solutal buoyancy effects are comparable in magnitude, and this gives rise to the distinctive layered structure. As illustrated in Fig. 3, the entire cavity is filled with the fully-established layers. It should be stressed that, if all the boundary walls were impermeable to solute transfer so that there were no sources or sinks of the solute on the boundaries, this layered flow structure could not persist in the quasi-steady state. However, as is the case for the present problem, owing to the continuous supply/removal of solute from the horizontal walls, the layered flow structure can sustain in the quasi-steady state. In conformity to the velocity field, the temperature field is stably stratified within the localized zone of the individual layer; the conductive mode prevails in the interfaces between the neighbouring layers. The solutal field exhibits the step-like variations in the vertical direction. Within each velocity layer, the solute is substantially uniform due to vigorous convective mixing within the cell. Large changes in solutal concentration take place at the interfaces. These prominent features of the thermal and solutal fields are qualitatively consistent with the well-documented characteristics pertaining to the layered structure of the classical double diffusive convection [1].

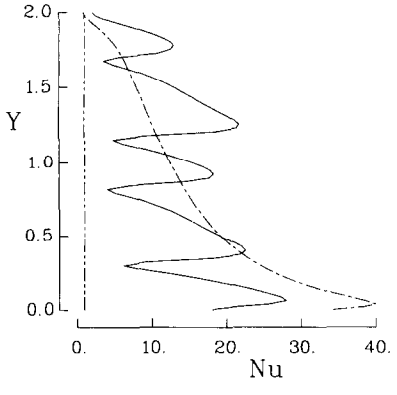

FIG. 5. Vertical profiles of the local Nu at $X = 0$. The values of R_ρ are: – – –, $R_\rho = 3.0$; ——, $R_\rho = 15.0$; – – – – –, $R_\rho = 50.0$.

The eminent flow features when R_ρ takes a very large value are displayed in Fig. 4 (for $R_\rho = 50.0$). In this case, the pre-existing stable solute stratification is predominant, and this inhibits thermal convection. Consequently, the flow in the major portion of the cavity is negligibly small in magnitude. Only in narrow localized regions adjacent to the horizontal walls are weak flows visible. Accordingly, the heat transfer is mostly controlled by conduction in the entire cavity, and the isotherms are substantially vertical. The solutal field shows a nearly-linear stratification in the vertical direction. The iso-solutal lines are slightly tilted downward; the horizontal density gradient caused by the temperature gradient is balanced by the solutal gradient, i.e.

$$\frac{\partial T}{\partial X} - R_\rho \frac{\partial S}{\partial X} \cong 0.$$

Utilizing the numerical data, the heat transfer rates at the heated sidewall, expressed by the local Nusselt number, $Nu = -\partial T/\partial X|_{X=0}$, are plotted in Fig. 5. When R_ρ is large, as ascertained earlier, the heat transfer in much of the cavity is mainly conductive; the values of Nu are very small and fairly uniform. For intermediate values of R_ρ, the distinctive layer structure prevails; the vertical distribution of Nu shows fluctuating profiles. The local maxima correspond to the mid-levels of the velocity layers, and the local minima to those of the interfaces. When R_ρ is small, the maximum of Nu occurs near the bottom wall, and Nu decreases rather monotonically upward, in a manner similar to a purely thermal convection.

4. CONCLUSION

Numerical solutions for double diffusive convection, subject to the externally-imposed horizontal temperature gradient and vertical solute gradient, are secured. Initiating from the pre-existing solutal stratification, large-time behaviour is elucidated as R_ρ encompasses a wide range.

Inspection of the large-time numerical solutions clearly points to the existence of three distinct flow regimes. When R_ρ is small, the overall flow properties are similar to those of a purely thermal convection. A unicell flow pattern is visible.

For moderate values of R_ρ, the distinguishing feature is the emergence of the multi-layered flow structure. When R_ρ is large, the fluid in the bulk of the container is essentially motionless, and heat transfer is mostly conductive.

The externally-imposed vertical solute gradient is responsible for generating these clearly definable flow regimes. The present findings are in qualitative agreement with the available experimental observations of ref. [9].

REFERENCES

1. S. A. Thorpe, P. K. Hutt and R. Soulsby, The effect of horizontal gradients on thermohaline convection, *J. Fluid Mech.* **38,** 375–400 (1969).
2. R. A. Wirtz and C. S. Reddy, Experiments on convective layer formation and merging in a differently heated slot, *J. Fluid Mech.* **91,** 451–464 (1979).
3. C. F. Chen, D. G. Briggs and R. A. Wirtz, Stability of thermal convection in a salinity gradient due to lateral heating, *Int. J. Heat Mass Transfer* **14,** 57–65 (1971).
4. H. E. Huppert and J. S. Turner, Ice blocks melting into a salinity gradient, *J. Fluid Mech.* **100,** 367–384 (1980).
5. H. E. Huppert, R. C. Kerr and A. Halworth, Heating or cooling a stable compositional gradient from the side, *Int. J. Heat Mass Transfer* **27,** 1395–1401 (1984).
6. R. A. Wirtz, D. G. Briggs and C. F. Chen, Physical and numerical experiments on layered convection in a density stratified fluid, *Geophys. Fluid Dyn.* **3,** 265–288 (1972).
7. S. Ostrach, Natural convection with combined driving forces, *PhysicoChem. Hydrodyn.* **1,** 233–247 (1980).
8. J. W. Lee and J. M. Hyun, Time-dependent double diffusion in a stably stratified fluid under lateral heating, *Int. J. Heat Mass Transfer* **34,** 2409–2421 (1991).
9. J. Lee, M. T. Hyun and Y. S. Kang, Confined natural convection due to lateral heating in a stably stratified solution, *Int. J. Heat Mass Transfer* **33,** 869–875 (1989).
10. S. V. Patankar, *Numerical Heat Transfer and Fluid Flow*. McGraw-Hill, New York (1980).
11. J. Patterson and J. Imberger, Unsteady natural convection in a rectangular cavity, *J. Fluid Mech.* **100,** 65–86 (1980).

Int. J. Heat Mass Transfer. Vol. 34, No. 9, pp. 2427–2430, 1991
Printed in Great Britain

0017–9310/91 $3.00 + 0.00
© 1991 Pergamon Press plc

Effect of spanwise spacing on the heat transfer from an array of protruding elements in forced convection

S. V. GARIMELLA† and P. A. EIBECK

Department of Mechanical Engineering, University of California at Berkeley, Berkeley, CA 94720, U.S.A.

(*Received* 13 *April* 1990 *and in final form* 26 *November* 1990)

INTRODUCTION

THE COOLING of an array of heat-generating elements mounted in a rectangular channel is an area of immediate interest in electronics packaging research. This problem constitutes a simulation of the flow passages between adjacent circuit boards carrying electronic chips in the CPU of a modern mainframe computer. The heat transfer coefficients as well as the flow patterns within the three-dimensional arrays of chips are not well understood. General surveys of the heat transfer problems in electronics cooling are presented in Chu [1] and Hannemann *et al.* [2], among others.

One topic of interest is the effect of spanwise spacing between elements of each row on the cooling that can be accomplished. Spanwise spacing as a parameter has not been investigated in the literature. Moffat *et al.* [3] studied the heat transfer from two array densities but did not specifically address the influence of spanwise spacing. The first results for liquid cooling of arrays of protruding elements with a range of inter-element spacings in the streamwise and spanwise directions were presented in ref. [4]. The heat transfer coefficient was shown to increase monotonically with an increase in streamwise spacing causing a spread of 35–40% in the heat transfer coefficient for a variation of streamwise spacing over the range of 0.5–6.5 element heights. In comparison, the spread was only 15% for an identical variation in the spanwise spacing between elements.

In the present study, the influence of the spanwise spacing between elements of an array on heat transfer and fluid dynamics is investigated in detail. The elements are mounted on the bottom wall of a horizontal water channel. Flow visualization using laser-sheet-illuminated hydrogen bubbles is used to document the flow patterns within the array.

EXPERIMENTS

A horizontal Plexiglas water channel with a cross section of 36.6 cm by 6.7 cm and a total length of 180.3 cm was used for the experiments. The height of the channel H was varied over 1.2, 1.9, 2.7, and 3.6 element heights. A schematic of the flow loop is shown in Fig. 1. A detailed description of the experimental facility and procedures is provided in ref. [4].

The bottom wall of the channel is equipped with two detachable hatches. The smaller upstream hatch holds a 25 μm nichrome wire strung spanwise to generate hydrogen

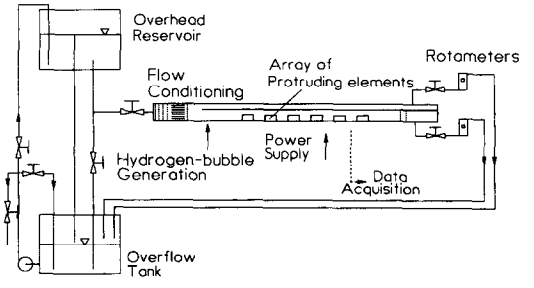

FIG. 1. Schematic of the liquid cooling test facility.

† Current address: Department of Mechanical Engineering, University of Wisconsin, Milwaukee, WI 53201, U.S.A.